Supplementary material: Uncertainty Based Camera Model Selection

Michal Polic
CTU in Prague*

Stanislav Steidl
CTU in Prague*

Zuzana Kukelova
CTU in Prague†

Cenek Albl
ETH Zurich

Tomas Pajdla
CTU in Prague*

1. Introduction

The supplementary material clarifies possible questions form the main paper and lists all the experiments which we could not handle in the main paper.

2. Camera model selection (ACS)

The ASC method propagates the uncertainty of input observations Σ_u into the accuracy of parameters which are common for all reconstructions $\hat{\boldsymbol{\theta}}^{(i)}$. We provide the visualization of the estimate of Σ_u in Figure 1.

*CIIRC - Czech Institute of Informatics, Robotics and Cybernetics, Czech Technical University in Prague, †Faculty of Electrical Engineering, Czech Technical University in Prague.

Figure 1: The estimation of affine shapes (green) using COLMAP [39] and the covariances (orange) of keypoints

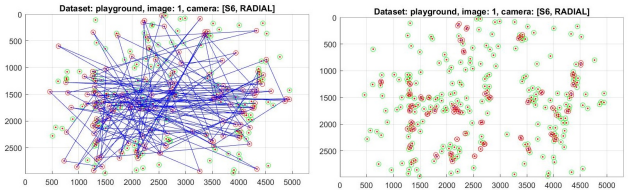

Figure 2: The example of the images with 50% of the outliers. Observations $\boldsymbol{u}$ (green/red circles for inliers/outliers) are connected with projections $\hat{\boldsymbol{u}}^{(i)}$ (red points) using blue lines. Left image shows random permutation of ids in $\boldsymbol{S}^{(i)}$. The right image shows systematic permutation of the closest observations

3. Description of IC

As the suitability of the mathematical model for given data is important task, large number of information criteria was derived. We compared 13 of them on the task of camera model selection. The ICs are summarized in Table 1 in the main paper. Here, we provide details about used notation. We assume model $\boldsymbol{M_i}$ in the following text and skip the $()^i$ index if it is clear from context.

We assumed the residuals has multivariate normal distribu-

#	Dataset	U	V	N
1	courtyard	38	33.5	360.4
2	delivery area	44	32.0	307.6
3	electro	45	20.3	285.3
4	facade	76	85.1	795.3
5	kicker	31	15.9	250.1
6	meadow	15	2.2	166.6
7	office	26	3.5	50.3
8	pipes	14	2.5	51.0
9	playground	38	15.7	361.7
10	relief	31	26.5	236.9
11	relief 2	31	20.5	176.4
12	terrace	23	10.7	190.6
13	terrains	42	18.5	254.4
14	terrains_rig	166	34.4	340.1
15	2011_09_26_drive_0001	114	-	-

Table 1: Summary of tested datasets. U is the number of images, V is the number of 3D points, and N is the number of observations assumed as inliers. V and N are in the table (written in thousands) if provided. Note that ETH datasets [40] provide 3D points that are not correctly aligned, and camera poses only are assumed as ground truth (GT). We are using these 3D points for the generation of synthetic datasets where the correct alignment is not necessary. The datasets (1-13) are ETH datasets [40] used for generation of synthetic reconstructions. The dataset 14 is ETH dataset with GT camera poses and datasets 15 is KITTI datasets without any information about GT

tion $\hat{\boldsymbol{e}}_{l,m} \in \mathcal{N}(0, \Sigma_{u_{l,m}})$. It leads to log-likelihood

$$L = -\frac{1}{2}\left(log(det(\Sigma_u)) + \hat{\boldsymbol{e}}^{\mathsf{T}}\Sigma_u^{-1}\hat{\boldsymbol{e}} + \mathcal{D}(\hat{\boldsymbol{e}}_{l,m})Nlog(2\pi)\right). \tag{1}$$

where Σ_u is the block-diagonal matrix composed of $\Sigma_{u_{l,m}}$ and $\hat{\boldsymbol{e}}$ vector of corresponding $\hat{\boldsymbol{e}}_{l,m}$. The dimension of residuals is $\mathcal{D}(\hat{\boldsymbol{e}}_{l,m}) = 2$ for the camera model selection and $\mathcal{D}(\widetilde{f}(\widetilde{x}) - \widetilde{y}) = 1$ for the problem of polynomial fitting. The determinant $\det(\Sigma_u)$ equals σ^{2N} in case of one dimensional residuals. The sum of all squared weighted residuals for tested camera model is

$$R = \sum_{(l,m)\in S} \hat{\boldsymbol{e}}_{l,m}^{\mathsf{T}}\Sigma_{u_{l,m}}^{-1}\hat{\boldsymbol{e}}_{l,m}. \tag{2}$$

"Constant term" (holds for constant N) of log-likelihood is

$$T = -\frac{1}{2}\log(\det(\Sigma_u)) - \frac{1}{2}\mathcal{D}(\hat{\boldsymbol{e}}_{l,m})N\log(2\pi) \tag{3}$$

and the log-likelihood for all observations is

$$L = T - R\,. \tag{4}$$

Further, we use the upper index R^{tal}, R^{hub} to distinguish between Talwar $\mathcal{L}_{tal}$ and Huber $\mathcal{L}_{hub}$ loss function $\mathcal{L}$. The lower index will correspond to camera model. The most complex camera model (from the set of candidates models $\mathcal{M}$) is denoted as $\bar{\boldsymbol{M}}$. Since R is a function depending on $u_{l,m}$ and $\hat{u}_{l,m}$, which are moreover for different models and inlier thresholds different, we will instead of $R(\boldsymbol{u}_{l,m}, \hat{\boldsymbol{u}}_{l,m})$ write $R(I_{\boldsymbol{M}})$. Here $I_{\boldsymbol{M}}$ is the index set of inliers $\boldsymbol{u}_{l,m}$ for model $\boldsymbol{M}$ and inlier threshold δ. For example

$$R^{tal}_{\bar{\boldsymbol{M}}}(I_{\boldsymbol{M}_{0|0}}) = \sum_{(l,m)\in I_{\boldsymbol{M}_{0|0}}} \mathcal{L}_{tal}(\hat{\boldsymbol{e}}_{(l,m),\bar{\boldsymbol{M}}}, \delta) \tag{5}$$

is the sum of squared residuals $\hat{\boldsymbol{e}}_{(l,m),\bar{\boldsymbol{M}}}$ for observations indexed by $I_{\boldsymbol{M}_{0|0}}$ and weighted by loss function $\mathcal{L}_{tal}$. Note that in this case the residuals are not generated for parameters of the model $\boldsymbol{M}_{0|0}$ but for parameters of $\bar{\boldsymbol{M}}$, i.e $\hat{\boldsymbol{u}}_{l,m}$ were obtained using projection function related to model $\bar{\boldsymbol{M}}$.

The variance $\sigma^2_{\bar{\boldsymbol{M}}}(I)$ of the set of inliers $I_{\boldsymbol{M}}$ of model $\boldsymbol{M}$ is computed from the residuals of the most complex model $\bar{\boldsymbol{M}}$, i.e. $\hat{\boldsymbol{e}}_{(l,m),\bar{\boldsymbol{M}}}$, as

$$\sigma^2_{\bar{\boldsymbol{M}}}(I) = \frac{R_{\bar{\boldsymbol{M}}}(I)}{\mathcal{D}(I) - k}\,. \tag{6}$$

The Talwar and the Huber loss functions are defined for threshold of reprojection error δ and reprojection error $\hat{\epsilon}_{l,m} = ||\hat{\boldsymbol{e}}_{l,m}||$ as

$$\mathcal{L}_{tal}(\hat{\epsilon}_{l,m}, \delta) = \begin{cases} \epsilon^2_{l,m}/2 & \text{if } |\hat{\epsilon}_{l,m}| \le \delta \\ \delta^2/2 & \text{if } |\hat{\epsilon}_{l,m}| > \delta \end{cases} \tag{7}$$

$$\mathcal{L}_{hub}(\hat{\epsilon}_{l,m}, \delta) = \begin{cases} \epsilon^2_i/2 & \text{if } |\hat{\epsilon}_{l,m}| \le \delta \\ \delta(|\hat{\epsilon}_{l,m}| - \delta/2) & \text{if } |\hat{\epsilon}_{l,m}| > \delta. \end{cases} \tag{8}$$

4. Experimental evaluation

This section provides the details about datasets, calibration parameters of physical cameras used for generation of synthetic scenes and show the examples of polynomials used in polynomial fitting task. We also provide detailed description of the experiment of polynomial fitting. Further, we show the visualisation of generated missmatches in experiment "the outliers filtering". At the end, the camera model selection on the tested models is summarized.

Datasets. The Table 1 summarize all the used datasets and their properties: number of images U, number of 3D points (in thousands) V and number of observations assumed as inliers (in thousands) N.

Physical cameras. The Table 16 and 17 provides the information about the calibration of each individual physical camera w.r.t. all the assumed camera models.

Polynomial model estimation is evaluated on Figure 3. We generated $10k$ polynomials $\widetilde{y} = \widetilde{f}(\widetilde{x}) + \widetilde{\epsilon}$ of each degree $\{1, 2, 3, 4\}$ and each standard deviation of $\widetilde{\epsilon} \in \mathcal{N}(0, \widetilde{\sigma}^2)$ where $\widetilde{\sigma}^2 = \{10^{-2}, 10^{-3}, 10^{-4}\}$. Each polynomial has coefficients from range $[-1.5,\ 1.5]$, so that, we see significant part of the polynomial in interval $\widetilde{x} \in [-5, 5]$, see example on Figure 3. Note that measurements does not contain any outliers. Our method ACS with mean success rate 94.1% is less depended on large measurement deviations. We used the measurements with Euclidean distance $||\widetilde{f}(\widetilde{x}) - \widetilde{y}||$ smaller than $4\widetilde{\sigma}^2$ for fitting the polynomial of tested degree. If we assumed all the measurements, we always (i.e., for $120k$ trials) got for higher or the same AC for polynomial models of smaller degree. This holds up to rounding errors and shows that if several models leads to the same number of inliers, the simplest model is selected.

The outlier filtering experiment use $4,5$M covariances $\Sigma_{u_{l,m}}$ of keypoints from 454 images of ETH datasets. The visualisation of reprojection errors after randomly and systematically permuted 3D point ids in $\boldsymbol{S}$ on Figure 2.

Camera model estimation on 1-13 datasets is in following tables. The reconstructions are from COLMAP [39] with assumption of 2px reprojection error threshold. $T_1[sec]$ is the time of registration of K cameras, $T_{all}[sec]$ is the runtime of SfM, U is number of registered cameras, V and N are number of 3D points and number of observations in thousands, $\frac{\sqrt{R}}{N}[px]$ means reprojection error and $Q[cm]$ is the mean distance of camera centers from the ground truth. Camera models $\boldsymbol{M}$ which exceed the deadline $T_d = \gamma T_1$ (we assumed $\gamma = 5$) for registering $K = 15$ cameras are red, the best values are bold and the model selected by

LACS is in a border

$\mathcal{M}$	T_1	T_{all}	U	V	N	$\frac{\sqrt{R}}{N}$	Q
$\boldsymbol{M_{0\|0}}$	37.3	105.6	36	14.8	51.3	1.3	35.7
$\boldsymbol{M_{1\|0}}$	36.4	102.6	36	**15.8**	61.8	1.3	11.2
$\boldsymbol{M_{2\|0}}$	**22.8**	**55.2**	**38**	15.5	74.2	0.7	3.8
$\boldsymbol{M_{3\|0}}$	22.9	59.2	**38**	15.5	74.2	**0.6**	3.8
$\boldsymbol{M_{4\|0}}$	26.8	70.7	**38**	15.5	73.9	**0.6**	3.8
$\boldsymbol{M_{1\|1}}$	–	371.6	–	–	–	–	–
$\boldsymbol{M_{2\|2}}$	28.6	73.9	**38**	15.7	**74.7**	**0.6**	**3.7**
$\boldsymbol{M_{3\|3}}$	41.3	139.9	**38**	**15.8**	74.9	**0.6**	3.8

Table 2: The evaluation of courtyard dataset

$\mathcal{M}$	T_1	T_{all}	U	V	N	$\frac{\sqrt{R}}{N}$	Q
$\boldsymbol{M_{0\|0}}$	27.0	83.0	**40**	**22.0**	71.8	1.3	58.0
$\boldsymbol{M_{1\|0}}$	23.6	81.4	**40**	**22.0**	74.6	1.2	18.5
$\boldsymbol{M_{2\|0}}$	**20.8**	**58.8**	**40**	21.8	90.0	**0.6**	2.6
$\boldsymbol{M_{3\|0}}$	24.7	66.9	**40**	21.8	89.9	**0.6**	**2.5**
$\boldsymbol{M_{4\|0}}$	22.6	64.1	**40**	**22.0**	**90.5**	**0.6**	**2.5**
$\boldsymbol{M_{1\|1}}$	–	126.3	13	6.2	18.3	1.0	13.5
$\boldsymbol{M_{2\|2}}$	26.8	82.9	**40**	21.7	89.7	**0.6**	**2.5**
$\boldsymbol{M_{3\|3}}$	52.7	175.2	**40**	21.7	89.7	**0.6**	**2.5**

Table 3: The evaluation of delivery area dataset

$\mathcal{M}$	T_1	T_{all}	U	V	N	$\frac{\sqrt{R}}{N}$	Q
$\boldsymbol{M_{0\|0}}$	44.0	106.6	38	13.1	45.2	1.2	24.1
$\boldsymbol{M_{1\|0}}$	21.0	72.9	38	14.1	51.1	1.2	3.2
$\boldsymbol{M_{2\|0}}$	**16.1**	**43.9**	39	15.5	64.5	0.8	**2.5**
$\boldsymbol{M_{3\|0}}$	17.1	48.9	**40**	15.5	64.6	0.8	2.9
$\boldsymbol{M_{4\|0}}$	17.7	53.5	**40**	15.6	65.0	0.8	2.8
$\boldsymbol{M_{1\|1}}$	-	163.9	–	–	–	–	–
$\boldsymbol{M_{2\|2}}$	20.8	60.4	**40**	**15.7**	**65.1**	0.8	2.7
$\boldsymbol{M_{3\|3}}$	66.7	222.0	30	11.6	42.2	**0.6**	**2.5**

Table 4: The evaluation of electro dataset

$\mathcal{M}$	T_1	T_{all}	U	V	N	$\frac{\sqrt{R}}{N}$	Q
$\boldsymbol{M_{0\|0}}$	47.8	385.0	67	49.4	208.0	1.4	18.9
$\boldsymbol{M_{1\|0}}$	50.0	315.3	67	**47.4**	228.1	1.3	5.6
$\boldsymbol{M_{2\|0}}$	**42.4**	**207.0**	74	46.5	272.1	0.8	5.5
$\boldsymbol{M_{3\|0}}$	43.6	214.4	74	46.5	271.6	**0.7**	5.4
$\boldsymbol{M_{4\|0}}$	49.1	246.6	74	46.7	**272.4**	**0.7**	5.5
$\boldsymbol{M_{1\|1}}$	–	1135.8	–	–	–	–	–
$\boldsymbol{M_{2\|2}}$	54.7	282.5	**75**	46.7	272.3	**0.7**	5.4
$\boldsymbol{M_{3\|3}}$	611.5	1324.7	19	15.0	69.3	1.2	**3.4**

Table 5: The evaluation of facade dataset

$\mathcal{M}$	T_1	T_{all}	U	V	N	$\frac{\sqrt{R}}{N}$	Q
$\boldsymbol{M_{0\|0}}$	35.9	62.6	**30**	9.1	32.0	1.3	7.0
$\boldsymbol{M_{1\|0}}$	26.9	56.8	**30**	**11.0**	41.0	1.3	2.6
$\boldsymbol{M_{2\|0}}$	**18.8**	**34.6**	**30**	10.9	**48.9**	**0.8**	**1.6**
$\boldsymbol{M_{3\|0}}$	20.2	37.8	**30**	10.8	48.5	**0.8**	**1.6**
$\boldsymbol{M_{4\|0}}$	20.7	39.9	**30**	10.7	48.4	**0.8**	**1.6**
$\boldsymbol{M_{1\|1}}$	-	198.4	–	–	–	–	–
$\boldsymbol{M_{2\|2}}$	24.6	47.8	**30**	10.7	48.2	**0.8**	**1.6**
$\boldsymbol{M_{3\|3}}$	126.6	192.8	**30**	10.8	48.5	0.9	**1.6**

Table 6: The evaluation of kicker dataset

$\mathcal{M}$	T_1	T_{all}	U	V	N	$\frac{\sqrt{R}}{N}$	Q
$\boldsymbol{M_{0\|0}}$	–	45.2	–	–	–	–	–
$\boldsymbol{M_{1\|0}}$	–	67.7	–	–	–	–	–
$\boldsymbol{M_{2\|0}}$	–	62.7	–	–	–	–	–
$\boldsymbol{M_{3\|0}}$	–	36.6	–	–	–	–	–
$\boldsymbol{M_{4\|0}}$	–	43.4	–	–	–	–	–
$\boldsymbol{M_{1\|1}}$	–	31.3	–	–	–	–	–
$\boldsymbol{M_{2\|2}}$	–	35.1	–	–	–	–	–
$\boldsymbol{M_{3\|3}}$	–	30.5	–	–	–	–	–

Table 7: The evaluation of meadow dataset

$\mathcal{M}$	T_1	T_{all}	U	V	N	$\frac{\sqrt{R}}{N}$	Q
$\boldsymbol{M_{0\|0}}$	9.2	11.5	18	1.4	4.6	1.3	3.5
$\boldsymbol{M_{1\|0}}$	9.0	12.9	**20**	1.8	6.8	1.2	2.2
$\boldsymbol{M_{2\|0}}$	**6.7**	**9.2**	**20**	1.8	**7.9**	**0.8**	0.9
$\boldsymbol{M_{3\|0}}$	6.9	11.0	**20**	1.8	7.8	**0.8**	0.8
$\boldsymbol{M_{4\|0}}$	8.9	13.3	**20**	**1.9**	**7.9**	**0.8**	**0.7**
$\boldsymbol{M_{1\|1}}$	–	56.4	–	–	–	–	–
$\boldsymbol{M_{2\|2}}$	23.3	26.6	**20**	1.8	**7.9**	**0.8**	**0.7**
$\boldsymbol{M_{3\|3}}$	–	78.5	–	–	–	–	–

Table 8: The evaluation of office dataset

$\mathcal{M}$	T_1	T_{all}	U	V	N	$\frac{\sqrt{R}}{N}$	Q
$\boldsymbol{M_{0\|0}}$	23.3	60.9	26	3.1	9.2	1.3	11.2
$\boldsymbol{M_{1\|0}}$	37.9	66.1	**29**	4.0	12.5	1.3	1.2
$\boldsymbol{M_{2\|0}}$	22.7	38.9	**29**	4.4	16.1	0.8	**0.5**
$\boldsymbol{M_{3\|0}}$	11.7	**22.4**	**29**	4.5	16.2	**0.7**	0.6
$\boldsymbol{M_{4\|0}}$	**9.3**	27.1	**29**	4.4	15.9	**0.7**	0.6
$\boldsymbol{M_{1\|1}}$	–	82.4	–	–	–	–	–
$\boldsymbol{M_{2\|2}}$	38.4	55.5	**29**	**4.6**	**16.3**	**0.7**	0.6
$\boldsymbol{M_{3\|3}}$	–	108.9	–	–	–	–	–

Table 9: The evaluation of playground dataset

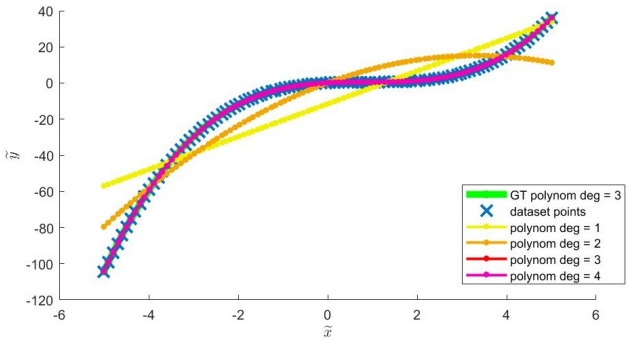

a) Example of fitted polynomial deg = 3

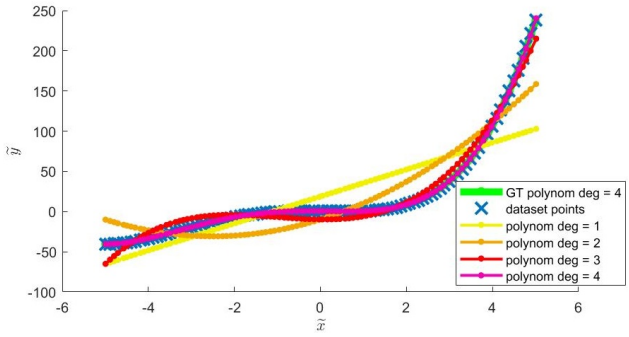

b) Example of fitted polynomial deg = 4

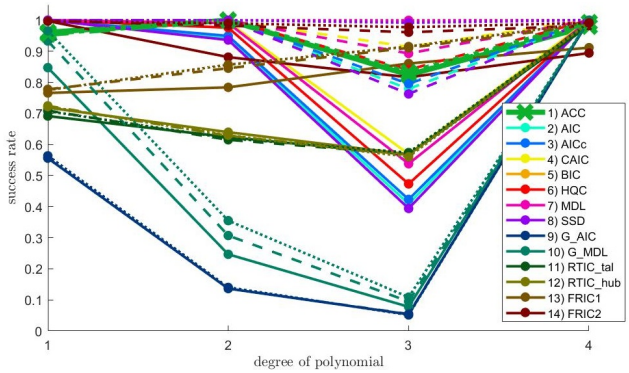

c) Figure 2 from the main paper

Figure 3: The comparison of success rate of correctly estimated degree of polynomial by ICs from Table 1 in the main paper. We visualize the examples of fitted polynomials. The polynomials $\widetilde{f}$, where $\widetilde{y} = \widetilde{f}(\widetilde{x}) + \widetilde{\epsilon}$. Each point in figure is computed from $10k$ trials. Each polynomial was fitted statistically optimal way form 100 measurements, where $\widetilde{x}$ was equally distributed in interval $\widetilde{x} \in [-5, 5]$ and measurements $\widetilde{y}$ was loaded with error $\widetilde{\epsilon} \in \mathcal{N}(0, \widetilde{\sigma}^2)$ where $\widetilde{\sigma}^2 = [10^{-2}, 10^{-3}, 10^{-4}]$ for [solid,dashed,dotted] line. The method ACS use $4\widetilde{\sigma}^2$ as the threshold for outliers, i.e, measurements with $||f(x) - y|| > 4\widetilde{\sigma}^2$ were not assumed for fitting

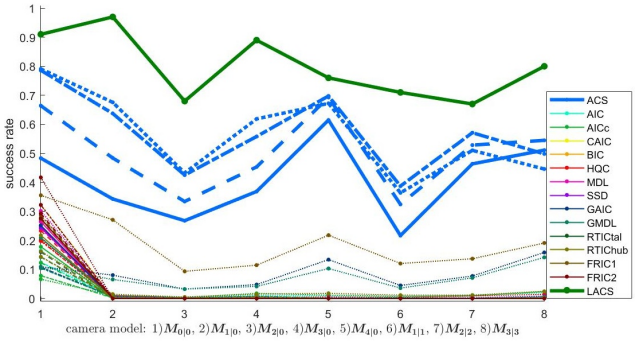

Figure 4: Comparison of the success rate of the information criteria for camera model selection task. The synthetical experiment with all the assumed camera models in real experiments, i.e., $\boldsymbol{M_{0|0}}$, $\boldsymbol{M_{1|0}}$, $\boldsymbol{M_{2|0}}$, $\boldsymbol{M_{3|0}}$, $\boldsymbol{M_{4|0}}$, $\boldsymbol{M_{1|1}}$, $\boldsymbol{M_{2|2}}$, $\boldsymbol{M_{3|3}}$. The lines {solid, long dashed, short dashed, doted} correspond to $\{0.5,\ 1,\ 1.5,\ 2\}$px of threshold for weighted reprojection error. LACS uses all thresholds

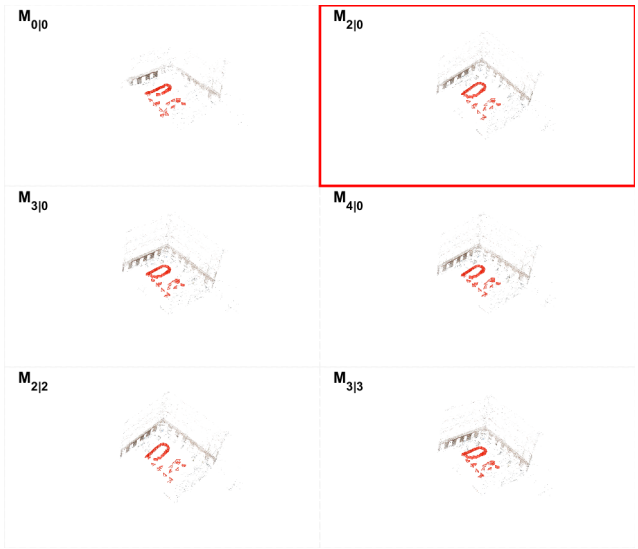

Figure 5: The 3D reconstructions of courtyard dataset.

$\mathcal{M}$	T_1	T_{all}	U	V	N	$\frac{\sqrt{R}}{N}$	Q
$\boldsymbol{M_{0\|0}}$	52.8	57.5	**18**	5.2	14.7	1.2	7.0
$\boldsymbol{M_{1\|0}}$	50.3	55.2	**18**	4.9	14.7	1.2	2.3
$\boldsymbol{M_{2\|0}}$	**44.4**	**47.3**	**18**	5.3	19.4	**0.6**	0.8
$\boldsymbol{M_{3\|0}}$	47.7	50.6	**18**	5.3	19.4	**0.6**	0.8
$\boldsymbol{M_{4\|0}}$	52.7	56.0	**18**	**5.7**	**20.0**	**0.6**	**0.7**
$\boldsymbol{M_{1\|1}}$	–	231.1	–	–	–	–	–
$\boldsymbol{M_{2\|2}}$	58.0	62.2	**18**	5.2	19.0	**0.6**	**0.7**
$\boldsymbol{M_{3\|3}}$	–	124.6	13	13.3	69.6	**0.6**	0.1

Table 10: The evaluation of relief dataset

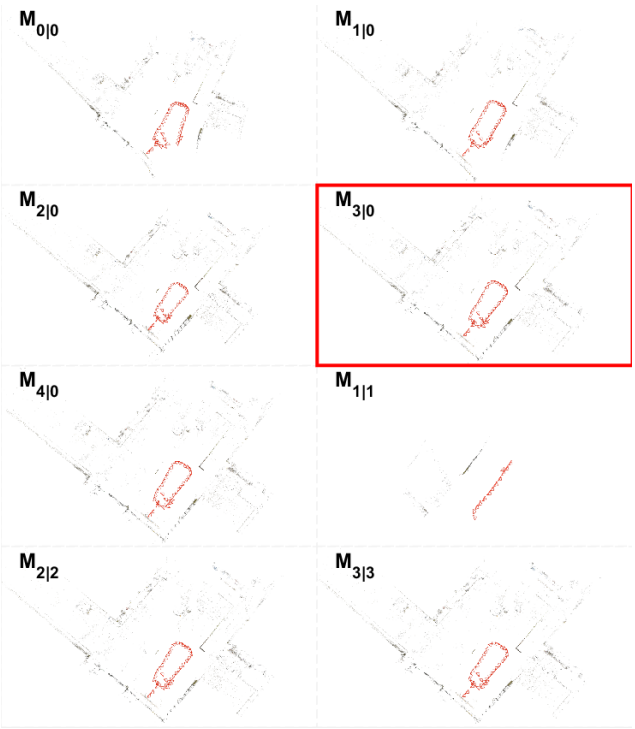

Figure 6: The 3D reconstructions of delivery area dataset.

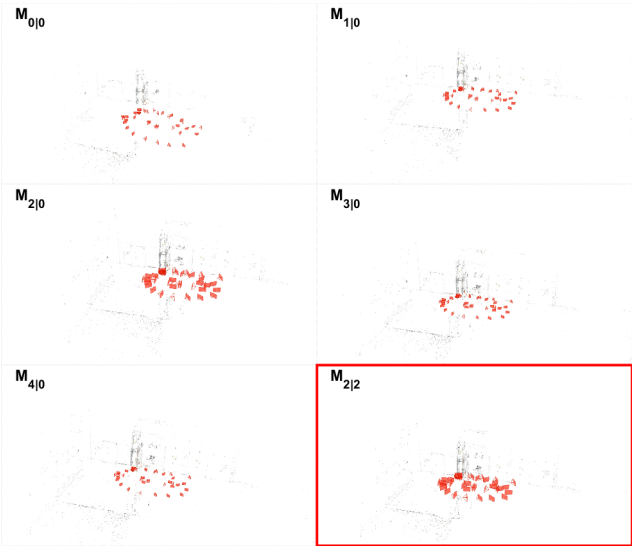

Figure 7: The 3D reconstructions of electro dataset.

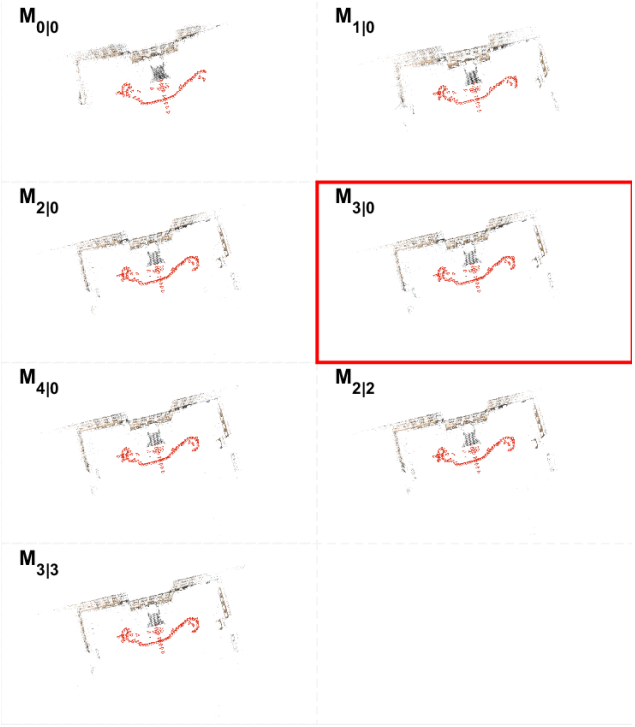

Figure 8: The 3D reconstructions of facade dataset.

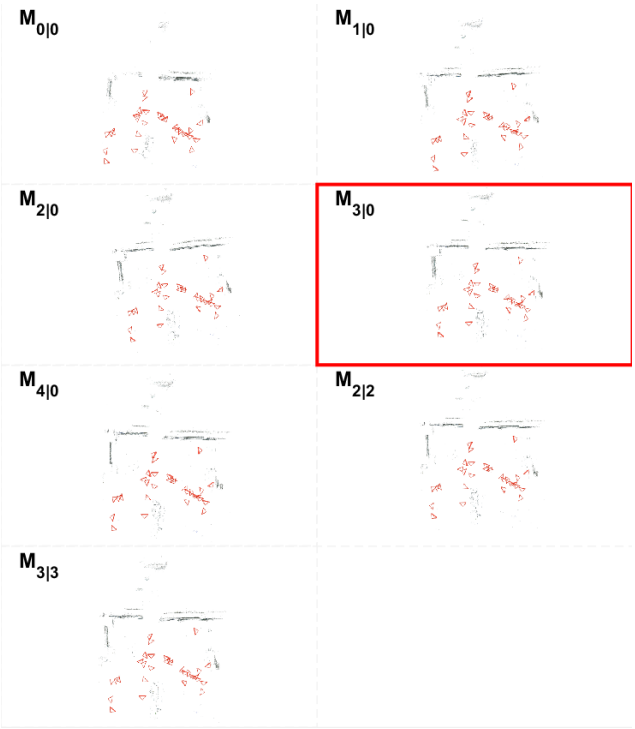

Figure 9: The 3D reconstructions of kicker dataset.

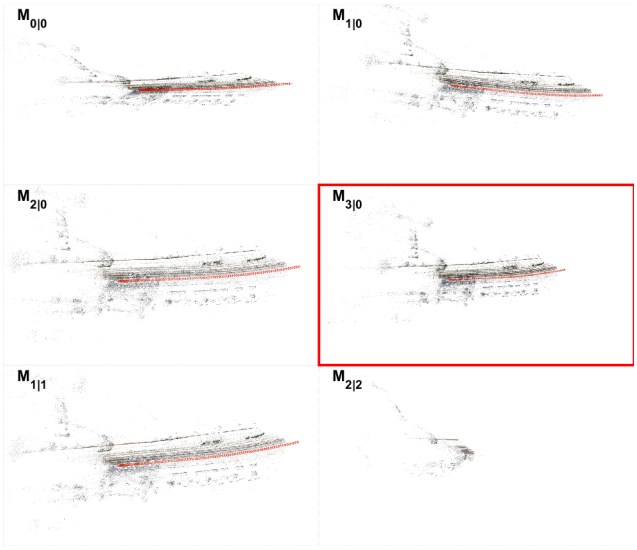

Figure 10: The 3D reconstructions of KITTI drive 0001 dataset.

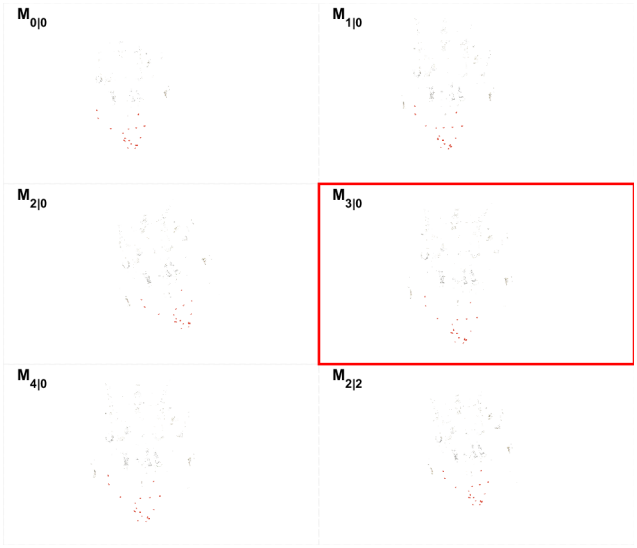

Figure 11: The 3D reconstructions of office dataset.

$\mathcal{M}$	T_1	T_{all}	U	V	N	$\frac{\sqrt{R}}{N}$	Q
$\boldsymbol{M_{0\|0}}$	47.3	55.4	**20**	5.3	17.1	1.2	6.4
$\boldsymbol{M_{1\|0}}$	41.3	50.3	**20**	5.3	17.6	1.2	4.9
$\boldsymbol{M_{2\|0}}$	**33.9**	**39.5**	**20**	**5.5**	**20.8**	0.6	**0.7**
$\boldsymbol{M_{3\|0}}$	38.6	53.3	**20**	4.9	17.6	0.6	29.7
$\boldsymbol{M_{4\|0}}$	37.5	50.0	**20**	5.1	17.8	**0.5**	28.4
$\boldsymbol{M_{1\|1}}$	–	221.9	–	–	–	–	–
$\boldsymbol{M_{2\|2}}$	50.1	57.9	**20**	**5.5**	**20.8**	0.6	**0.7**
$\boldsymbol{M_{3\|3}}$	–	100.3	13	3.2	11.3	0.6	0.5

Table 11: The evaluation of relief 2 dataset

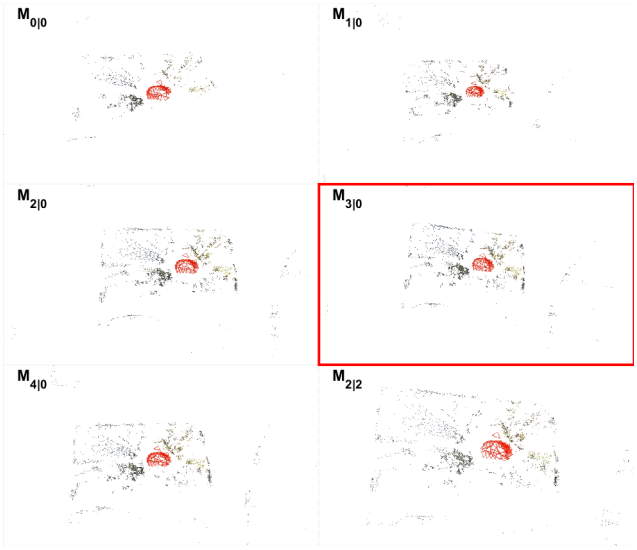

Figure 12: The 3D reconstructions of playground dataset.

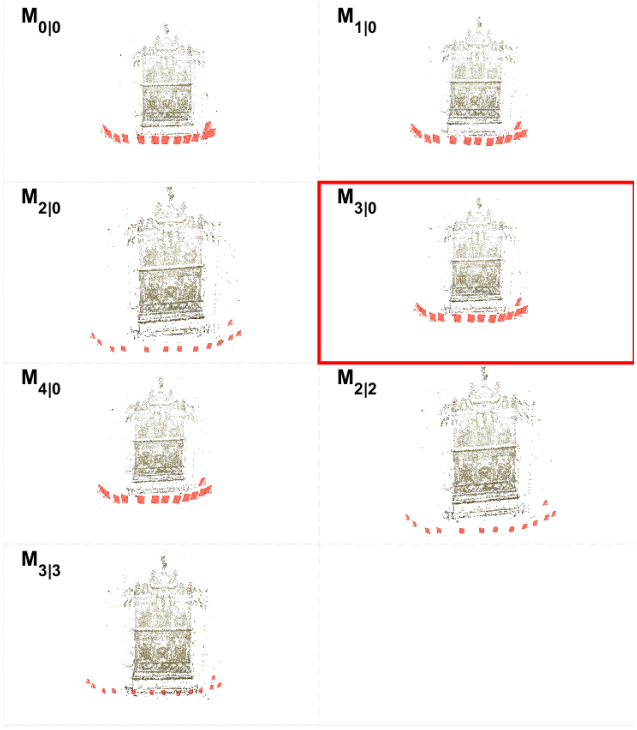

Figure 13: The 3D reconstructions of relief dataset.

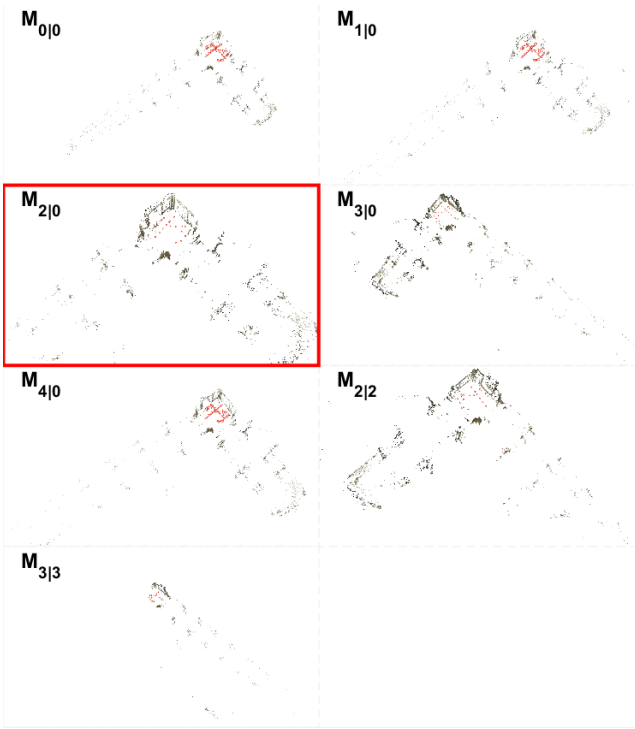

Figure 14: The 3D reconstructions of relief 2 dataset.

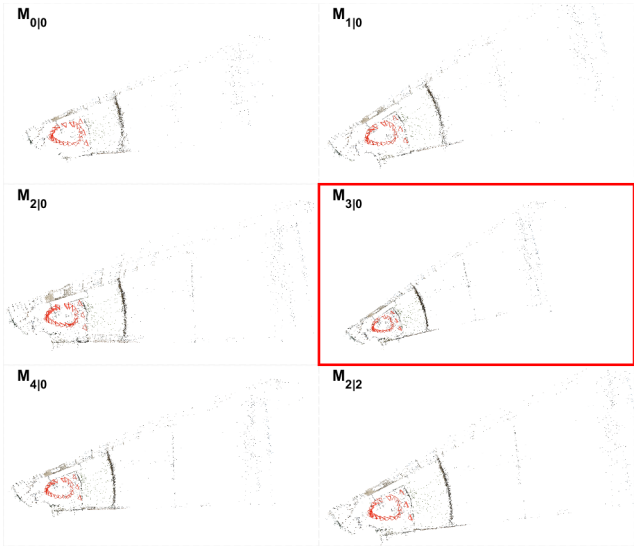

Figure 15: The 3D reconstructions of terrace dataset.

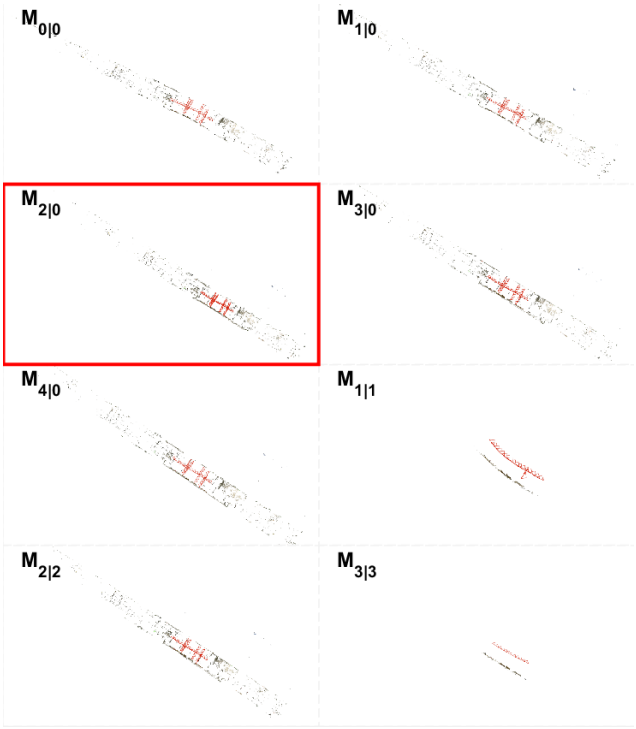

Figure 16: The 3D reconstructions of terrains dataset.

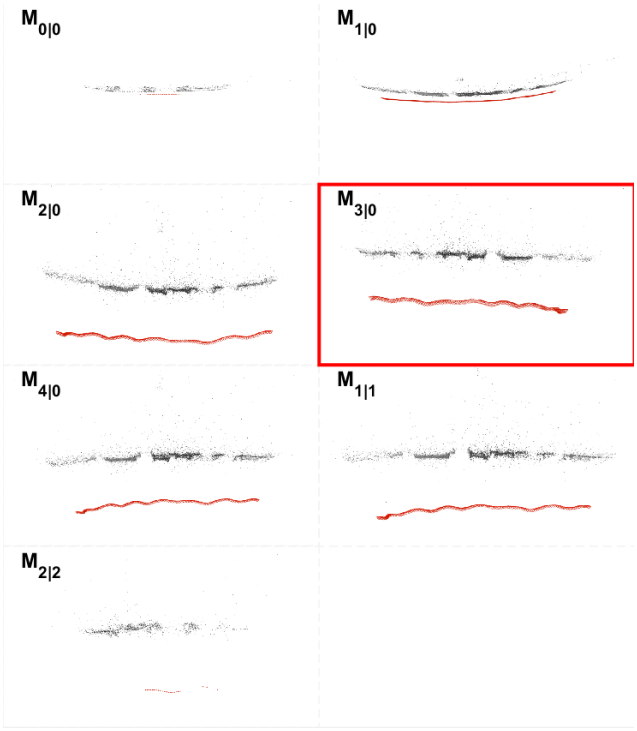

Figure 17: The 3D reconstructions of terrains rig dataset.

$\mathcal{M}$	T_1	T_{all}	U	V	N	$\frac{\sqrt{R}}{N}$	Q
$\boldsymbol{M_{0\|0}}$	18.7	35.2	**23**	6.9	22.0	1.4	22.2
$\boldsymbol{M_{1\|0}}$	19.0	33.7	**23**	7.3	26.3	1.3	1.7
$\boldsymbol{M_{2\|0}}$	15.3	23.7	**23**	7.4	30.1	**0.8**	**1.5**
$\boldsymbol{M_{3\|0}}$	**14.6**	**23.3**	**23**	7.4	30.0	**0.8**	1.6
$\boldsymbol{M_{4\|0}}$	15.7	24.9	**23**	**7.5**	**30.2**	**0.8**	1.6
$\boldsymbol{M_{1\|1}}$	–	95.4	–	–	–	–	–
$\boldsymbol{M_{2\|2}}$	20.2	31.4	**23**	7.3	29.7	**0.8**	1.7
$\boldsymbol{M_{3\|3}}$	–	118.6	–	–	–	–	–

Table 12: The evaluation of terrace dataset

$\mathcal{M}$	T_1	T_{all}	U	V	N	$\frac{\sqrt{R}}{N}$	Q
$\boldsymbol{M_{0\|0}}$	61.9	129.3	**42**	15.6	52.4	1.1	11.6
$\boldsymbol{M_{1\|0}}$	71.2	144.8	**42**	16.0	54.6	1.1	6.8
$\boldsymbol{M_{2\|0}}$	**22.2**	53.5	**42**	**16.1**	**66.4**	**0.6**	**0.5**
$\boldsymbol{M_{3\|0}}$	23.2	**51.4**	**42**	16.0	66.0	**0.6**	**0.5**
$\boldsymbol{M_{4\|0}}$	25.1	59.7	**42**	15.9	65.9	**0.6**	**0.5**
$\boldsymbol{M_{1\|1}}$	40.9	56.1	19	10.3	39.6	0.7	7.0
$\boldsymbol{M_{2\|2}}$	30.0	69.7	**42**	**16.1**	**66.4**	**0.6**	**0.5**
$\boldsymbol{M_{3\|3}}$	63.0	286.4	17	4.9	17.0	**0.6**	0.3

Table 13: The evaluation of terrains dataset

$\mathcal{M}$	T_1	T_{all}	U	V	N	$\frac{\sqrt{R}}{N}$	Q
$\boldsymbol{M_{0\|0}}$	**7.0**	1070.2	34	6.7	64.1	0.7	2.5
$\boldsymbol{M_{1\|0}}$	32.0	626.8	**165**	**17.5**	210.5	0.9	7.0
$\boldsymbol{M_{2\|0}}$	16.9	212.7	**165**	**17.5**	**210.9**	0.8	6.4
$\boldsymbol{M_{3\|0}}$	17.6	175.7	**165**	17.3	210.2	0.7	3.1
$\boldsymbol{M_{4\|0}}$	29.5	215.1	**165**	17.2	209.6	0.7	3.7
$\boldsymbol{M_{1\|1}}$	12.0	**172.3**	**165**	17.2	209.6	0.7	3.5
$\boldsymbol{M_{2\|2}}$	94.7	1443.8	**165**	17.3	210.1	0.8	3.7
$\boldsymbol{M_{3\|3}}$	83.4	1545.0	18	4.3	27.0	**0.5**	**0.8**

Table 14: The evaluation of terrains rig dataset

$\mathcal{M}$	T_1	T_{all}	U	V	N	$\frac{\sqrt{R}}{N}$	Q
$\boldsymbol{M_{0\|0}}$	113.5	1323.6	**114**	34.4	305.4	0.8	–
$\boldsymbol{M_{1\|0}}$	91.7	1401.3	**114**	52.3	424.2	0.6	–
$\boldsymbol{M_{2\|0}}$	**84.2**	1407.1	**114**	64.7	502.7	0.6	–
$\boldsymbol{M_{3\|0}}$	105.7	**1272.2**	**114**	**66.2**	**504.5**	0.6	–
$\boldsymbol{M_{4\|0}}$	-	2238.4	–	–	–	–	–
$\boldsymbol{M_{1\|1}}$	206.1	1628.0	**114**	64.7	496.7	0.6	–
$\boldsymbol{M_{2\|2}}$	-	**431.2**	12	7.6	104.8	**0.4**	–
$\boldsymbol{M_{3\|3}}$	-	1543.2	–	–	–	–	–

Table 15: The evaluation of 2011_09_26_drive_0001 KITTI dataset

Table 16: Physical cameras 1/2

Sony A3500 [5456 × 3632]px										
$\mathcal{M}$	$\hat{f}$	$\hat{pp}_1$	$\hat{pp}_2$	$\hat{k}_1$	$\hat{k}_2$	$\hat{k}_3$	$\hat{k}_4$	$\hat{d}_1$	$\hat{d}_2$	$\hat{d}_3$
$\boldsymbol{M_{0\|0}}$	4263.1	2742.5	1829.8	-	-	-	-	-	-	-
$\boldsymbol{M_{1\|0}}$	4180.4	2726.4	1810.8	−0.033	-	-	-	-	-	-
$\boldsymbol{M_{2\|0}}$	4180.4	2724.4	1811.6	−0.057	0.049	-	-	-	-	-
$\boldsymbol{M_{3\|0}}$	4180.4	2724.3	1811.5	−0.056	0.045	0.007	-	-	-	-
$\boldsymbol{M_{4\|0}}$	4181.6	2723.8	1811.5	−0.065	0.125	−0.264	0.303	-	-	-
$\boldsymbol{M_{1\|1}}$	4180.8	2725.0	1812.3	1.778	-	-	-	1.845	-	-
$\boldsymbol{M_{2\|2}}$	4181.1	2723.7	1811.7	−0.695	−2.399	-	-	−0.634	−2.518	-
$\boldsymbol{M_{3\|3}}$	4291.7	2731.1	1848.3	−0.053	0.233	0.888	-	0.239	0.217	1.014

Canon G16 [2816 × 2112]px										
$\mathcal{M}$	$\hat{f}$	$\hat{pp}_1$	$\hat{pp}_2$	$\hat{k}_1$	$\hat{k}_2$	$\hat{k}_3$	$\hat{k}_4$	$\hat{d}_1$	$\hat{d}_2$	$\hat{d}_3$
$\boldsymbol{M_{0\|0}}$	2343.1	1410.6	1079.4	-	-	-	-	-	-	-
$\boldsymbol{M_{1\|0}}$	2343.2	1406.0	1059.1	−0.028	-	-	-	-	-	-
$\boldsymbol{M_{2\|0}}$	2343.8	1406.0	1059.5	−0.031	0.010	-	-	-	-	-
$\boldsymbol{M_{3\|0}}$	2344.3	1406.1	1059.7	−0.035	0.036	−0.049	-	-	-	-
$\boldsymbol{M_{4\|0}}$	2344.3	1406.1	1059.7	−0.034	0.030	−0.026	−0.031	-	-	-
$\boldsymbol{M_{1\|1}}$	2343.9	1406.0	1059.5	0.357	-	-	-	0.389	-	-
$\boldsymbol{M_{2\|2}}$	2344.3	1406.1	1059.7	−0.653	−1.767	-	-	−0.618	−1.820	-
$\boldsymbol{M_{3\|3}}$	2350.7	1407.8	1056.1	−0.025	0.046	0.352	-	−0.067	0.077	0.366

Creative Web Camera [1280 × 720]px										
$\mathcal{M}$	$\hat{f}$	$\hat{pp}_1$	$\hat{pp}_2$	$\hat{k}_1$	$\hat{k}_2$	$\hat{k}_3$	$\hat{k}_4$	$\hat{d}_1$	$\hat{d}_2$	$\hat{d}_3$
$\boldsymbol{M_{0\|0}}$	1112.1	607.1	351.4	-	-	-	-	-	-	-
$\boldsymbol{M_{1\|0}}$	1105.0	612.7	357.2	−0.028	-	-	-	-	-	-
$\boldsymbol{M_{2\|0}}$	1105.0	612.8	357.2	−0.027	−0.002	-	-	-	-	-
$\boldsymbol{M_{3\|0}}$	1101.7	610.4	359.8	0.043	−0.486	0.944	-	-	-	-
$\boldsymbol{M_{4\|0}}$	1101.2	610.3	359.5	0.071	−0.824	2.418	−2.123	-	-	-
$\boldsymbol{M_{1\|1}}$	1105.0	612.8	357.2	−0.064	-	-	-	−0.037	-	-
$\boldsymbol{M_{2\|2}}$	1102.1	610.9	359.3	−7.347	33.132	-	-	−7.366	33.310	-
$\boldsymbol{M_{3\|3}}$	1101.4	610.4	359.5	0.316	3.743	21.133	-	0.257	4.329	20.205

GoPro Hero4 [4000 × 3000]px										
$\mathcal{M}$	$\hat{f}$	$\hat{pp}_1$	$\hat{pp}_2$	$\hat{k}_1$	$\hat{k}_2$	$\hat{k}_3$	$\hat{k}_4$	$\hat{d}_1$	$\hat{d}_2$	$\hat{d}_3$
$\boldsymbol{M_{0\|0}}$	1758.3	2028.4	1393.1	-	-	-	-	-	-	-
$\boldsymbol{M_{1\|0}}$	1759.5	2073.0	1471.0	−0.098	-	-	-	-	-	-
$\boldsymbol{M_{2\|0}}$	1759.0	1926.2	1483.2	−0.216	0.044	-	-	-	-	-
$\boldsymbol{M_{3\|0}}$	1750.5	1962.8	1514.0	−0.240	0.059	−0.006	-	-	-	-
$\boldsymbol{M_{4\|0}}$	1749.4	1961.7	1492.3	−0.251	0.074	−0.012	0.001	-	-	-
$\boldsymbol{M_{1\|1}}$	1752.2	1999.8	1487.4	0.146	-	-	-	0.407	-	-
$\boldsymbol{M_{2\|2}}$	1750.9	1933.3	1464.4	0.453	0.013	-	-	0.731	0.073	-
$\boldsymbol{M_{3\|3}}$	1751.0	1933.3	1464.4	0.374	−0.032	−0.002	-	0.653	0.005	−0.008

Table 17: Physical cameras 2/2

Samsung S10e, camera 0 [4032 × 3024]px										
$\mathcal{M}$	$\hat{f}$	$\hat{pp}_1$	$\hat{pp}_2$	$\hat{k}_1$	$\hat{k}_2$	$\hat{k}_3$	$\hat{k}_4$	$\hat{d}_1$	$\hat{d}_2$	$\hat{d}_3$
$\boldsymbol{M_{0\|0}}$	3239.0	2004.0	1561.4	-	-	-	-	-	-	-
$\boldsymbol{M_{1\|0}}$	3250.4	1996.8	1561.0	−0.024	-	-	-	-	-	-
$\boldsymbol{M_{2\|0}}$	3246.4	1995.2	1558.0	−0.013	−0.029	-	-	-	-	-
$\boldsymbol{M_{3\|0}}$	3208.2	1997.9	1554.0	0.143	−0.802	1.112	-	-	-	-
$\boldsymbol{M_{4\|0}}$	3179.9	2005.0	1555.3	0.365	−2.719	7.405	−6.800	-	-	-
$\boldsymbol{M_{1\|1}}$	3249.2	1995.8	1559.6	−0.454	-	-	-	−0.433	-	-
$\boldsymbol{M_{2\|2}}$	3189.0	2002.7	1552.8	−7.909	111.498	-	-	−8.088	111.486	-
$\boldsymbol{M_{3\|3}}$	3172.8	2004.8	1557.5	0.036	2.599	52.382	-	2.753	2.165	53.779

Samsung S10e, camera 1 [4608 × 3456]px										
$\mathcal{M}$	$\hat{f}$	$\hat{pp}_1$	$\hat{pp}_2$	$\hat{k}_1$	$\hat{k}_2$	$\hat{k}_3$	$\hat{k}_4$	$\hat{d}_1$	$\hat{d}_2$	$\hat{d}_3$
$\boldsymbol{M_{0\|0}}$	1832.9	2281.2	1709.5	-	-	-	-	-	-	-
$\boldsymbol{M_{1\|0}}$	1826.3	2279.8	1713.0	−0.008	-	-	-	-	-	-
$\boldsymbol{M_{2\|0}}$	1815.8	2282.5	1712.3	0.014	−0.017	-	-	-	-	-
$\boldsymbol{M_{3\|0}}$	1817.1	2282.8	1712.4	0.010	−0.012	−0.002	-	-	-	-
$\boldsymbol{M_{4\|0}}$	1823.1	2282.9	1712.5	−0.019	0.058	−0.063	0.018	-	-	-
$\boldsymbol{M_{1\|1}}$	1815.2	2282.1	1715.6	−0.380	-	-	-	−0.373	-	-
$\boldsymbol{M_{2\|2}}$	1819.4	2283.0	1712.3	−1.058	0.367	-	-	−1.060	0.371	-
$\boldsymbol{M_{3\|3}}$	1814.9	2282.7	1711.4	0.013	−0.016	0.000	-	0.000	0.000	0.000

Samsung S6 [5312 × 2988]px										
$\mathcal{M}$	$\hat{f}$	$\hat{pp}_1$	$\hat{pp}_2$	$\hat{k}_1$	$\hat{k}_2$	$\hat{k}_3$	$\hat{k}_4$	$\hat{d}_1$	$\hat{d}_2$	$\hat{d}_3$
$\boldsymbol{M_{0\|0}}$	3991.5	2639.6	1538.9	-	-	-	-	-	-	-
$\boldsymbol{M_{1\|0}}$	4014.2	2644.5	1583.0	0.033	-	-	-	-	-	-
$\boldsymbol{M_{2\|0}}$	4008.3	2649.6	1570.5	0.157	−0.411	-	-	-	-	-
$\boldsymbol{M_{3\|0}}$	4004.8	2647.1	1569.6	0.184	−0.620	0.453	-	-	-	-
$\boldsymbol{M_{4\|0}}$	4010.0	2647.8	1569.2	0.127	0.136	−3.197	5.747	-	-	-
$\boldsymbol{M_{1\|1}}$	4001.5	2641.6	1593.6	14.916	-	-	-	14.521	-	-
$\boldsymbol{M_{2\|2}}$	4011.2	2647.2	1568.8	−3.342	20.556	-	-	−3.455	20.723	-
$\boldsymbol{M_{3\|3}}$	4016.6	2646.7	1574.2	0.189	16.929	103.273	-	−12.841	16.983	97.871

Apple iPhone SE [4032 × 3024]px										
$\mathcal{M}$	$\hat{f}$	$\hat{pp}_1$	$\hat{pp}_2$	$\hat{k}_1$	$\hat{k}_2$	$\hat{k}_3$	$\hat{k}_4$	$\hat{d}_1$	$\hat{d}_2$	$\hat{d}_3$
$\boldsymbol{M_{0\|0}}$	3513.7	2013.8	1499.5	-	-	-	-	-	-	-
$\boldsymbol{M_{1\|0}}$	3451.8	2027.8	1522.3	0.075	-	-	-	-	-	-
$\boldsymbol{M_{2\|0}}$	3453.4	2027.2	1522.0	0.067	0.041	-	-	-	-	-
$\boldsymbol{M_{3\|0}}$	3460.1	2023.7	1520.9	−0.008	0.937	−2.996	-	-	-	-
$\boldsymbol{M_{4\|0}}$	3463.1	2023.2	1520.1	−0.055	1.914	−10.366	18.050	-	-	-
$\boldsymbol{M_{1\|1}}$	3453.0	2027.4	1522.1	−0.314	-	-	-	−0.383	-	-
$\boldsymbol{M_{2\|2}}$	3463.4	2023.2	1519.9	1.269	75.669	-	-	1.325	74.179	-
$\boldsymbol{M_{3\|3}}$	3466.2	2022.7	1520.2	0.070	14.967	20.889	-	−5.447	15.095	17.886